The Astrophysical Journal, 688:24–31, 2008 November 20

TRIS. II. SEARCH FOR CMB SPECTRAL DISTORTIONS AT 0.60, 0.82, AND 2.5 GHz

M. Gervasi,[1,2] M. Zannoni,[1] A. Tartari, G. Boella,[2] and G. Sironi[1]
Physics Department, University of Milano Bicocca, I20126 Milan, Italy; mario.zannoni@mib.infn.it
Received 2007 October 3; accepted 2008 July 28

ABSTRACT

With the TRIS experiment we have performed absolute measurements of the sky brightness in a sky circle at $\delta = +42^\circ$ at the frequencies $\nu = 0.60$, 0.82, and 2.5 GHz. In this paper we discuss the techniques used to separate the different contributions to the sky emission and give an evaluation of the absolute temperature of the CMB. For the blackbody temperature of the CMB we get $T^{\rm th}_{\rm CMB} = 2.837 \pm 0.129 \pm 0.066$ K at $\nu = 0.60$ GHz, $T^{\rm th}_{\rm CMB} = 2.803 \pm 0.051\,^{+0.430}_{-0.300}$ K at $\nu = 0.82$ GHz, and $T^{\rm th}_{\rm CMB} = 2.516 \pm 0.139 \pm 0.284$ K at $\nu = 2.5$ GHz. The first error bar is statistic (1 σ), while the second one is systematic. These results represent a significant improvement with respect to the previous measurements. We have also set new limits to the free-free distortions, $-6.3 \times 10^{-6} < Y_{\rm ff} < 12.6 \times 10^{-6}$, and slightly improved the Bose-Einstein upper limit, $|\mu| < 6 \times 10^{-5}$, both at 95% confidence level.

Subject headings: cosmic microwave background — cosmological parameters — cosmology: observations — diffuse radiation — radio continuum: galaxies

1. INTRODUCTION

At decimetric wavelengths the sky brightness temperature ($T_{\rm sky}$) can be written as the sum of different contributions: cosmic microwave background (CMB; $T_{\rm CMB}$), Galactic emission ($T_{\rm Gal}$), and unresolved extragalactic radio sources (UERSs; $T_{\rm UERS}$).

The temperature of the CMB, $T_{\rm CMB}$, can be considered, for our purposes, as isotropic. The largest anisotropy component is the dipole term $\Delta T_{\rm dipole}(\alpha, \delta) = T_d \cos\theta$, with $T_d = 3.381 \pm 0.007$ mK and θ angle between the direction of observation and the maximum of the dipole at ($\alpha = 11^{\rm h}12.2^{\rm m} \pm 0.8^{\rm m}$, $\delta = -7.06^\circ \pm 0.16^\circ$) (Bennet et al. 1996; Fixen et al. 1996; Fixen & Mather 2002). It gives a level of anisotropy well inside the error budget of our absolute measurements. Therefore, we consider in the present paper only the possible dependence of the CMB brightness temperature on the frequency [$T_{\rm CMB}(\nu)$]. The frequency dependence could be related to the spectral distortion of the CMB.

The most accurate measurement of the CMB temperature so far made is the one obtained by the *COBE* FIRAS team (Mather et al. 1990, 1994, 1999; Fixen et al. 1996; Fixen & Mather 2002). Between 60 and 600 GHz they found a spectrum fully compatible with a blackbody emitting at the thermodynamic temperature $T^{\rm th}_{\rm CMB} = 2.725 \pm 0.001$ K (see Fixen & Mather 2002). Major spectral distortions in this range are excluded by *COBE* FIRAS, and the parameters of both the Bose-Einstein (BE) and Compton distortions are largely constrained: $|\mu| < 9 \times 10^{-5}$ and $|y| < 15 \times 10^{-6}$ (both at 95% CL; see Fixen et al. 1996).

Although very accurate, the FIRAS result covers only part of the CMB frequency spectrum. In particular, it does not cover the low-frequency region where TRIS measurements were made and where distortions can be expected. Table 1 collects the measurements of the CMB temperature made at frequencies below a few GHz starting from the 1980s. At these low frequencies the error bars are much larger than at FIRAS frequencies, essentially because of the large uncertainties associated with the absolute calibration procedures and with the presence of important foregrounds.

To improve the low-frequency situation, it has been proposed in the past to carry on measurements of the CMB temperature from space: LOBO (Sironi et al. 1995, 1997), for which TRIS is a pathfinder, and DIMES (Kogut 1996). DIMES has been then transformed into a balloon program (ARCADE), whose results have been published recently (see Kogut et al. 2004; Fixen et al. 2004; Singal et al. 2006).

The blackbody spectrum of the CMB is the result of the complete thermalization of the universe in the prerecombination era. At that time the strong interactions among the different components of the cosmic plasma were efficient enough to reestablish immediately the thermodynamic equilibrium after an energy injection. Nevertheless, small deviations from the blackbody distribution can survive if the energy injection occurred at a redshift $z \lesssim 10^6$. In the prerecombination era ($z \gtrsim 10^4$–10^3) a kinetic equilibrium is reestablished through the Compton scattering, double Compton scattering, and the bremsstrahlung mechanism. The resulting spectrum assumes a typical shape described by the BE or the Compton distribution. For a review of these mechanisms see Zel'dovich & Sunyaev (1969), Sunyaev & Zel'dovich (1970, 1980), Zel'dovich et al. (1972), and Illarionov & Sunyaev (1975a, 1975b), while detailed calculations have been performed by Burigana et al. (1991a, 1991b, 1995) and Daly (1991). These types of distortions are described by the chemical potential μ and the Comptonization parameter y, whose possible values have been already limited by *COBE* FIRAS.

Energy injections after the recombination era are responsible for spectral distortions without any possibility of rethermalization. Among these processes there is the photon injection through the free-free (FF) mechanism in a reionized universe (see Bartlett & Stebbins 1991). This effect depends on the square of the wavelength and therefore is dominant at very low frequencies and is not constrained by the *COBE* FIRAS measurements. Other possible distortions are related to the formation of primordial molecules and to the formation of structures at large scale. Both these mechanisms are difficult to model, but, at least in the case of the formation of primordial molecules, a not negligible effect could be expected at decimetric wavelengths (see Varshalovich & Khersonskii 1977; Dubrovich & Stolyarov 1995).

The Galactic emission [$T_{\rm Gal}(\nu, \alpha, \delta)$] is anisotropic and has a power-law frequency spectrum: $T_{\rm Gal}(\nu) = T_{\rm Gal}(\nu_0)(\nu/\nu_0)^\beta$. Its importance and properties are analyzed in Tartari et al. (2008, hereafter Paper III), from which we take the spectral index β we use in the following.

[1] Also Italian National Institute for Astrophysics, INAF, Milan, Italy.
[2] Also Italian National Institute for Nuclear Physics, INFN, Milano-Bicocca, Italy.

TABLE 1
A Summary of Low-Frequency CMB Absolute Temperature Measurements Collected Starting from the 1980s

λ (cm)	ν (GHz)	$T_{\rm CMB}$ (K)	References
50.0	0.60	3.0 ± 1.2	1
36.6	0.82	2.7 ± 1.6	2
23.4	1.28	3.45 ± 0.78	3
21.3	1.41	2.11 ± 0.38	4
21.05	1.425	$2.65^{+0.33}_{-0.30}$	5
20.4	1.47	2.26 ± 0.19	6
15.0	2.0	2.55 ± 0.14	7
12.0	2.5	2.62 ± 0.25	8
12.0	2.5	2.79 ± 0.15	9
12.0	2.5	2.50 ± 0.34	2
8.1	3.7	2.59 ± 0.13	10
7.9	3.8	2.56 ± 0.08	11
7.9	3.8	2.71 ± 0.07	11
7.9	3.8	2.64 ± 0.07	12
6.3	4.75	2.71 ± 0.20	13
6.3	4.75	2.70 ± 0.07	14

References.— (1) Sironi et al. 1990; (2) Sironi et al. 1991; (3) Raghunathan & Subrahmanyan 2000; (4) Levin et al. 1988; (5) Staggs et al. 1996; (6) Bensadoun et al. 1993; (7) Bersanelli et al. 1994; (8) Sironi et al. 1984; (9) Sironi & Bonelli 1986; (10) De Amici et al. 1988; (11) De Amici et al. 1990; (12) De Amici et al. 1991; (13) Mandolesi et al. 1984; (14) Mandolesi et al. 1986.

The contribution of the UERSs, $T_{\rm UERS}$, has also a power-law frequency spectrum, but for a low-resolution experiment it can be considered isotropic. In the following we take it from the model developed by Gervasi et al. (2008) on the basis of the source number count measurements available in literature.

After a brief summary of the TRIS experiment (§ 2), in § 3 we discuss the techniques used to separate the components of $T_{\rm sky}$ and the results obtained for $T_{\rm CMB}$. The implications of these results in terms of spectral distortions are presented in § 4.

2. TRIS

The TRIS experiment, fully described in Zannoni et al. (2008, hereafter Paper I), is a set of three absolute total power radiometers. They were operated (1996–2000) at Campo Imperatore (Italy), a site at 2000 m a.s.l. where a reasonable compromise of radio quietness, winter accessibility, and heavy logistics was achieved. After a few tests to minimize the effects of the radio frequency interferences, the radiometers were tuned at $\nu =$ 0.60050, 0.81785, and 2.42775 GHz. All the radiometers had the same block diagram (see Fig. 1). The antennas, rectangular horns corrugated on the E-plane, were geometrically scaled and had the same beam size [18° (E) $\times$ 23° (H) HPBW] with sidelobes lower than -40 dB. Two modes of observations were used: drift-scan mode and absolute measurement mode. During the drift scans the receivers were connected to the horn by a room-temperature waveguide-to-coaxial transition. During absolute measurements, the radiometers' front ends were cooled at liquid helium temperature, as shown in Figure 1.

2.1. *Drift Scans*

Most of the experiment lifetime was used to carry on drift scans of the sky with the antennas aimed at the zenith ($\delta = +42^\circ$). To avoid Sun contamination and keep the gain variation under control, the sky profiles were built using only data collected at nighttime, when the temperature stability of the receivers was better than $\pm 0.1^\circ$C. Receiver gain and change of the antenna impedance matching were checked at regular time intervals using the internal calibrator (IntCal block in Fig. 1), based on a noise source with a stability better than $\sim$0.1% over months. Data collected in rainy and cloudy conditions were rejected from the analysis (for details see §§ 4.2 and 4.4 of Paper I).

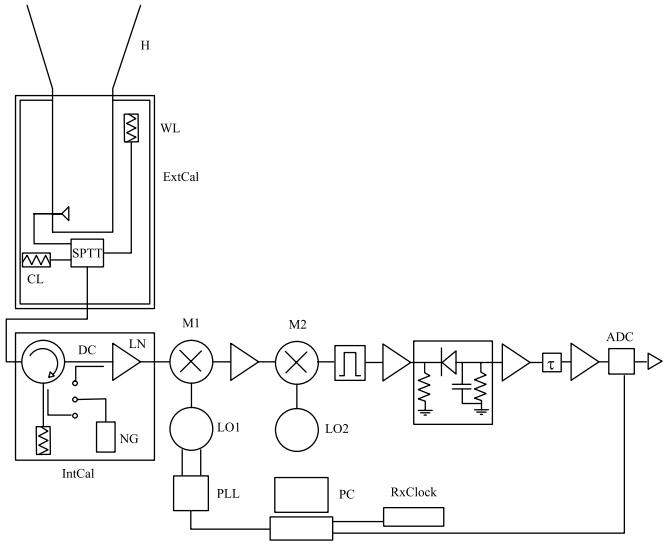

Fig. 1.— Schematic of TRIS antennas and receivers. The setup of the absolute measurements using the cryogenic front end is shown. The internal calibrator block (IntCal) is also shown. This schematic is the same at the three frequencies (0.60, 0.82, and 2.5 GHz) of the TRIS experiment.

Once properly combined, the TRIS drift scans give complete profiles of $T_{\rm sky}$ versus the right ascension α, along the circle at declination $\delta = +42^\circ$ at 0.60 and 0.82 GHz. At 2.5 GHz the level of radio frequency interferences hampered the construction of a complete profile. The error budget on the variations of the temperature along the profiles at 0.60 and 0.82 GHz is dominated by the uncertainties on the corrections for drifts and offsets and by the uncertainty in the determination of the temperature scale. In particular, at $8^{\rm h} \lesssim \alpha \lesssim 16^{\rm h}$, the Galactic halo region, which has been observed redundantly, an uncertainty on temperature variations in the range from 5 to 10 mK was achieved, at both 0.60 and 0.82 GHz. At $\alpha \sim 20^{\rm h}$ (see Fig. 2), the Galactic disk region, the larger uncertainty we obtained is due to the smaller number of drift scans. In drift-scan mode of observation (shown in Fig. 2) the zero level of the scale of temperature is arbitrary.

2.2. *Absolute Measurements*

During the absolute measurement campaigns, the radiometers were equipped with the cryogenic front end. The horns were attached to stainless steel waveguides and brass waveguide-to-coaxial transition, which were immersed in liquid helium to reduce their thermal emissions. Each cryostat housed also a single pole triple throw (SPTT; Fig. 1) passive resonant switch. The SPTT connects, for absolute calibration, the receiver alternately with the antenna or two reference dummy loads: cold load (CL) at $\sim$4 K and warm load (WL) at $\sim$270 K. Typical calibration runs, involving cold and warm loads and the internal calibration mark (CM), are shown in Figure 3. The transfer function of all the components between the horn mouth and the switch output (waveguides, transitions, cables, etc.) has been measured in laboratory. The only parts we were unable to measure are the flares of the horns: their attenuation has been calculated. Accurate measurements of the temperature profiles of these components, both inside and outside the cryostat, during the observations, combined with the attenuation, allow us to evaluate and subtract their contribution to the receiver output. At 0.82 GHz a failure of the dewar

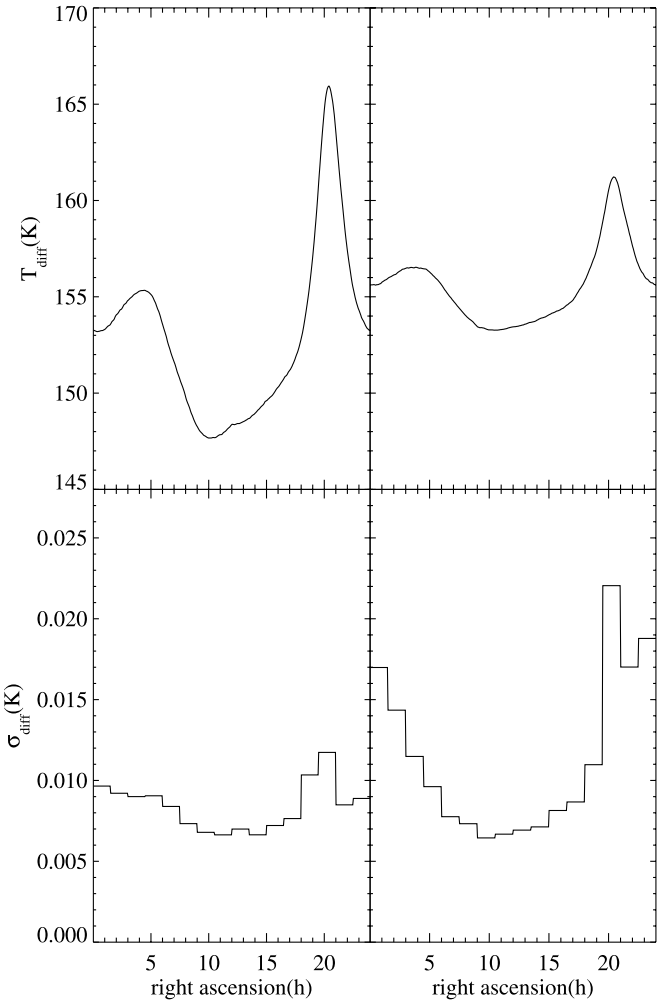

FIG. 2.—Drift-scan profiles at 0.60 and 0.82 GHz, with arbitrary zero level. The reported uncertainties represent the statistical error bar, which is the result of the collection of a large number of single drift-scan measurements.

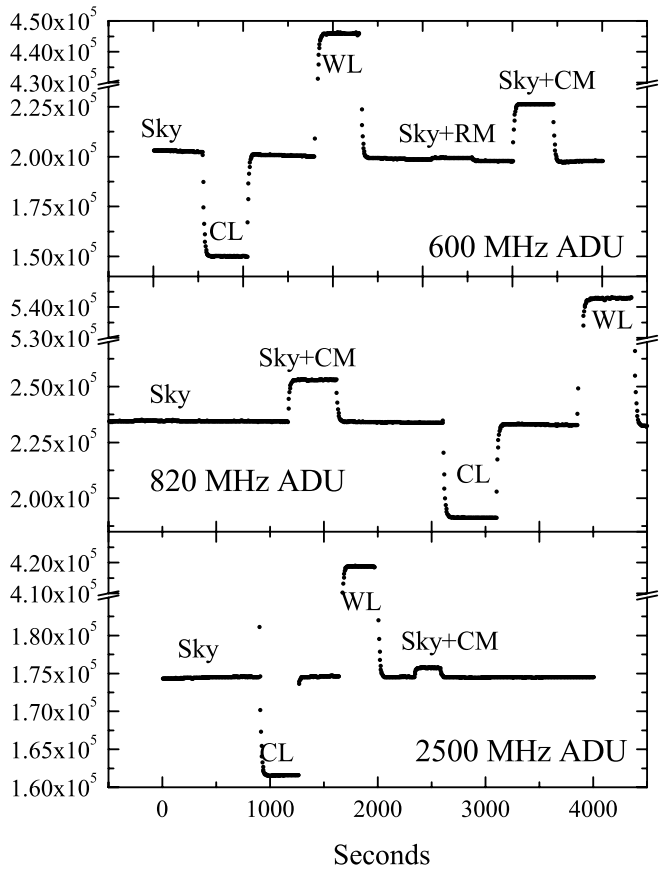

FIG. 3.—Typical run of absolute measurements at the three frequencies of TRIS. We measured the sky (Sky), the cold load (CL), the warm load (WL), the internal calibration mark (Sky+CM), and the impedance matching (Sky+RM). Signals are still in arbitrary digital units (ADU).

housing the cryogenic front end during absolute measurements forced us to use an alternative setup with only the SPTT switch cooled in liquid helium. This is the reason why the 0.82 GHz values of the sky temperature have a higher systematic uncertainty (for details see §§ 4.2 and 4.3 of Paper I).

Comparing the signals measured looking at the sky with the signals produced by the warm and cold loads, we get absolute values of the antenna temperature at various points along the circle at $\delta = +42^\circ$. Subtracting the environmental contribution (ground, atmosphere, radio frequency interferences), we get absolute values of the sky temperature at the same points. Details of this procedure are given in Paper I (§ 4.3.1), while results are presented in Table 2. The ground contribution has been calculated convolving the antenna beam with a blackbody at 290 K having the profile of the horizon at Campo Imperatore. The atmospheric transmission and emission have been evaluated using the model described in Ajello et al. (1995). The effect of radio frequency interferences has been evaluated by using metal shields around the horns. At 0.60 and 0.82 GHz they were well inside the system noise. At 2.5 GHz they were so frequent and strong that observations were possible only rarely (for details see Paper I).

The sky temperature values (T_{sky}) measured during the absolute observations were used to set the zero level of the drift scans. As a matter of fact, the drift scans, once reduced to the top of the atmosphere, had the same dynamic range of the absolute measurement data. In this way we got the absolute sky temperature also for those regions of the sky not observed during the absolute measurements. Table 3 reports the final accuracy of the absolute values of T_{sky}. The systematic uncertainty on the zero level quoted in Table 3 (ΔT_{zero}) applies also to the drift-scan profiles once corrected for the zero level. In Table 3 the number of independent sky positions analyzed during the absolute measurements is also shown.

3. SEPARATION OF THE COMPONENTS OF T_{sky}

At TRIS frequencies the brightness temperature of the sky can be written as

$$T_{sky}(\nu, \alpha) = T_{CMB}(\nu) + T_{Gal}(\nu, \alpha) + T_{UERS}(\nu). \quad (1)$$

TABLE 2

LOCAL CONTRIBUTION TO THE ANTENNA TEMPERATURE IN THE TRIS EXPERIMENT

Parameter	$\nu_0 = 0.60$ GHz	$\nu_0 = 0.82$ GHz	$\nu_0 = 2.5$ GHz
T_{atm} (K)	1.088 ± 0.023	1.221 ± 0.016	1.570 ± 0.025
$e^{-\tau_{atm}}$	0.995 ± 0.001	0.995 ± 0.001	0.993 ± 0.001
T_{ground} (K)	$0.07^{+0.06}_{-0.03}$	$0.07^{+0.06}_{-0.03}$	$0.07^{+0.06}_{-0.03}$
T_{RFI} (K)	<0.01	<0.01	9.82 ± 0.26

NOTE.—Atmospheric emission was evaluated by using a model (Ajello et al. 1995); ground contribution was evaluated convolving the ground profile with the antenna side lobes; radio frequency interferences were directly measured.

TABLE 3

ACCURACY OF THE ABSOLUTE MEASUREMENTS OF T_{sky} PERFORMED BY TRIS AT $\delta = +42^\circ$

ν (GHz)	ΔT_{stat} (mK)	ΔT_{zero} (mK)	Number of Sky Positions
0.60.....	18	66	34
0.82.....	32	$^{+430}_{-300}$[a]	12
2.5.....	10	284	6

[a] The zero-level uncertainty at 0.82 GHz coming from the absolute calibration is $\Delta T_{zero} = 659$ mK. The quoted value comes after astrophysical assumption on the Galactic signal (see Paper III, § 3).

The contribution (T_{UERS}) of UERSs at the TRIS frequencies can be obtained from Gervasi et al. (2008) and immediately subtracted from T_{sky}. The values we used are summarized in Table 4.

To disentangle T_{CMB} and T_{Gal} at 0.60 and 0.82 GHz, we take advantage of the accurate TRIS profiles of T_{sky} versus α (see § 3.1). At 2.5 GHz, because no drift scan is available, we followed a different approach (see § 3.2).

3.1. *Analysis of the Measurements at* 0.60 *and* 0.82 GHz

3.1.1. *The Position Difference Technique (PDT)*

The separation of the components of T_{sky} is possible because it is made of an isotropic component (T_{CMB} and T_{UERS}) plus an anisotropic component (T_{Gal}). The profiles of T_{sky} measured by TRIS at 0.60 and 0.82 GHz give the variation of T_{sky} with the right ascension α along a circle at constant declination ($\delta = +42^\circ$). We can take a pair of positions in the sky (α_1, α_2) at the two frequencies $\nu_1 = 0.60$ GHz and $\nu_2 = 0.82$ GHz and write a set of linear equations:

$$\begin{aligned}
T_{sky}(\nu_1, \alpha_1) - T_{UERS}(\nu_1) &= T_{CMB}(\nu_1) + T_{Gal}(\nu_1, \alpha_1),\\
T_{sky}(\nu_1, \alpha_2) - T_{UERS}(\nu_1) &= T_{CMB}(\nu_1) + T_{Gal}(\nu_1, \alpha_2),\\
T_{sky}(\nu_2, \alpha_1) - T_{UERS}(\nu_2) &= T_{CMB}(\nu_2) + T_{Gal}(\nu_2, \alpha_1),\\
T_{sky}(\nu_2, \alpha_2) - T_{UERS}(\nu_2) &= T_{CMB}(\nu_2) + T_{Gal}(\nu_2, \alpha_2). \quad (2)
\end{aligned}$$

The Galactic signal depends on both α and ν, and we can write

$$T_{Gal}(\nu, \alpha) = T_{Gal}(\nu_0, \alpha)\left(\frac{\nu}{\nu_0}\right)^{\beta(\alpha, \nu, \nu_0)}. \quad (3)$$

In spite of this simple analytical form, also the spectral index $\beta(\alpha, \nu, \nu_0)$ depends on α and ν. Putting $\nu_1 = \nu_0$ and taking the difference between pairs of equation (2), we get

$$\begin{aligned}
T_{sky}(\nu_1, \alpha_1) - T_{sky}(\nu_1, \alpha_2) &= T_{Gal}(\nu_1, \alpha_1) - T_{Gal}(\nu_1, \alpha_2),\\
T_{sky}(\nu_2, \alpha_1) - T_{sky}(\nu_2, \alpha_2) &= T_{Gal}(\nu_1, \alpha_1)m(\alpha_1)\\
&\quad - T_{Gal}(\nu_1, \alpha_2)m(\alpha_2), \quad (4)
\end{aligned}$$

with $m(\alpha) = (\nu_2/\nu_1)^{\beta(\alpha)}$. We can use these equations to separate the microwave sky components if we can find two positions α_1 and α_2 such that $\beta(\alpha_1) \neq \beta(\alpha_2)$ [$m(\alpha_1) \neq m(\alpha_2)$], $T_{sky}(\nu_1, \alpha_1) \neq T_{sky}(\nu_1, \alpha_2)$, and $T_{sky}(\nu_2, \alpha_1) \neq T_{sky}(\nu_2, \alpha_2)$. When these conditions, necessary to break the degeneracy, are satisfied, from equation (4) follows

$$\begin{aligned}
&\left[T_{sky}(\nu_2, \alpha_1) - T_{sky}(\nu_2, \alpha_2)\right]\\
&-\left[T_{sky}(\nu_1, \alpha_1) - T_{sky}(\nu_1, \alpha_2)\right]m(\alpha_1)\\
&\quad = T_{Gal}(\nu_1, \alpha_2)[m(\alpha_1) - m(\alpha_2)], \quad (5)
\end{aligned}$$

TABLE 4

CONTRIBUTION OF THE UNRESOLVED EXTRAGALACTIC RADIO SOURCES TO THE SKY BRIGHTNESS TEMPERATURE AT THE FREQUENCIES OF THE TRIS EXPERIMENT

ν (GHz)	T_{UERS} (mK)
0.60.....	934 ± 24
0.82.....	408 ± 10
2.50.....	22 ± 1

an equation we can use to extract T_{Gal}, if $m(\alpha_1)$ and $m(\alpha_2)$ are known. If m is unknown, we can look for different pairs of points close to α_1 and α_2, respectively, write a system of equations, and extract $T_{Gal}(\alpha)$ and $m(\alpha)$. Finally, going back to equation (2), we can get a number of values of $T_{CMB}(\nu)$ in the sky regions around α_1 and α_2.

3.1.2. *TT-Plot Technique*

For each pair of sky positions α_i and α_j, around α_1 and α_2, respectively, we can write

$$m(\alpha_{i,j}) = \frac{T_{sky}(\nu_2, \alpha_i) - T_{sky}(\nu_2, \alpha_j)}{T_{sky}(\nu_1, \alpha_i) - T_{sky}(\nu_1, \alpha_j)}. \quad (6)$$

In principle, one can repeat this procedure for all the pairs of points along the drift-scan profiles at 0.60 and 0.82 GHz obtained by TRIS, look for regions where the conditions to break the degeneracy are satisfied, and get m.

This can be done very efficiently using a well-known graphical method, the TT-plot technique, which allows one to look for correlation between the sky temperatures at two frequencies ν_1 and ν_2. Introduced by Turtle et al. (1962) and widely used also recently, e.g., in Davies et al. (1996) and Platania et al. (1998) to analyze maps of the microwave sky, it allows one to find regions where the values of m (and β) are well defined. These "homogeneous" regions can be selected by plotting $T_{sky}(\nu_2, \alpha)$ versus $T_{sky}(\nu_1, \alpha)$: all the positions α inside these regions distribute themselves along a straight line whose slope is m. This means that in these positions the spectral index can be considered uniform: $\beta(\alpha_i) \simeq \beta(\alpha_j)$.

As evident from equation (6), the values of $m(\alpha)$ [and $\beta(\alpha)$] obtained depend only on the temperature variations and are not affected by uncertainties on the zero level of the two scales of temperature (ΔT_{zero}). In § 3 of Paper III the TT-plot method has been applied to the TRIS profiles at 0.60 and 0.82 GHz (shown in Fig. 2). It shows that, along the circle at $\delta = +42^\circ$, there are two regions where the spectral indices are well defined and different: here the conditions to solve equation (5) apply. These two regions are $9^h \lesssim \alpha_1 \lesssim 11^h$, the halo region at the highest Galactic latitude, and $20^h \lesssim \alpha_2 \lesssim 21^h$, the Galactic disk, close to the Cygnus region.

3.1.3. *Monte Carlo Analysis*

Having the above information, we can now solve the equation and get T_{CMB} and T_{Gal} at various α. We did it by a Monte Carlo simulation. In this way we take directly into account the effects of the uncertainties, both statistic and systematic, of the measured quantities [$T_{sky}(\nu, \alpha)$] on the evaluation of the unknown quantities. We also assumed as prior the information coming from the TT-plot method used in Paper III, i.e., central value and width of the distribution of the spectral index $\beta(\alpha)$. Following this approach, we obtained the distribution of the values of $T_{CMB}(\nu_1)$ and $T_{CMB}(\nu_2)$, which include the effect of the distribution of all

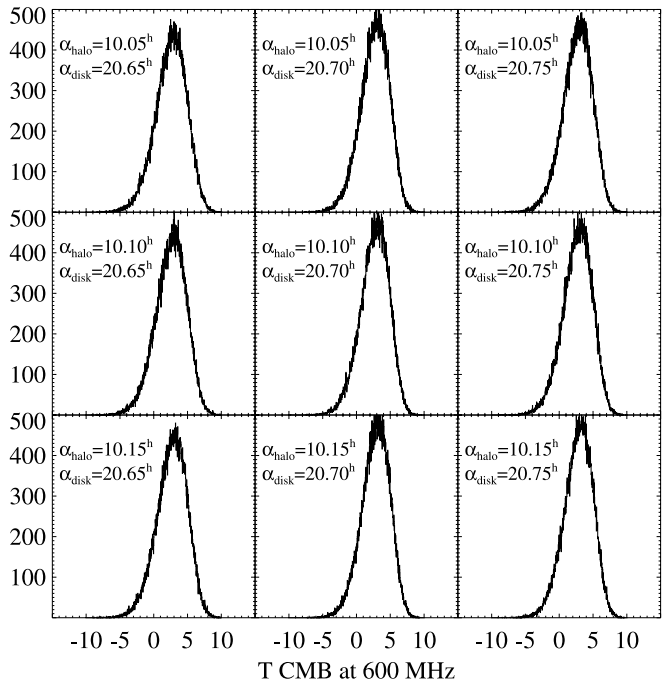

FIG. 4.—Brightness temperature of CMB evaluated with the position difference technique at 0.60 and 0.82 GHz. We got values from 288 pairs of position in the sky (32 positions in the halo times 9 positions in the disk). Here we show the Monte Carlo realizations in nine samples of sky position pairs.

the parameters involved in equation (2). The error bars of $T_{\rm CMB}$ have been evaluated by using the bootstrap method. The systematic uncertainty of the zero level of $T_{\rm sky}$ ($\Delta T_{\rm zero}$ in Table 3), not included in the MC analysis, has been quoted separately.

The values of $T_{\rm CMB}$ we obtained are distributed around a well-defined central value, as shown in Figure 4 and summarized in Table 5. We have also obtained the Galactic emission in the halo and disk regions (see Table 6). As shown by the system of equations given by equation (4), the absolute temperature of the Galaxy,

TABLE 5

BRIGHTNESS TEMPERATURE OF CMB AT 0.60 AND 0.82 GHz EVALUATED USING THE PDT METHOD AND THE SPECTRAL INDEX β OBTAINED WITH THE TT-PLOT TECHNIQUE AS PRIOR IN THE MONTE CARLO SIMULATIONS

ν (GHz)	$T_{\rm CMB}$ (K)	$\Delta T_{\rm zero}$ (K)	$\Delta T_{\rm MC}$ (K)
0.60	2.823	0.066	0.129
0.82	2.783	$^{+0.430}_{-0.300}$	0.051

evaluated using this method, is not affected by the systematic uncertainty ($\Delta T_{\rm zero}$) on the zero level of $T_{\rm sky}$.

3.1.4. *Graphic Method*

In principle, graphic methods can be used also to extract $T_{\rm CMB}$ from a TT-plot. Through each point $[T_{\rm sky}(\nu_1, \alpha); T_{\rm sky}(\nu_2, \alpha)]$, at a certain value of α, of the TT-plot we can draw a straight line of slope $m(\alpha) = (\nu_2/\nu_1)^{\beta(\alpha)}$ whose intercept T_0 is

$$T_0 = T_{\rm sky}(\nu_1, \alpha) - T_{\rm sky}(\nu_2, \alpha)\frac{1}{m(\alpha)}. \quad (7)$$

After simple algebra and assuming $T_{\rm CMB}(\nu_1) \equiv T_{\rm CMB}(\nu_2) = \overline{T_{\rm CMB}}$, we get

$$\overline{T_{\rm CMB}} = \frac{m}{m-1} \times \left[T_{\rm sky}(\nu_1) - T_{\rm sky}(\nu_2)\frac{1}{m} - T_{\rm UERS}(\nu_1)\left(1 - \frac{q}{m}\right)\right], \quad (8)$$

with $q = T_{\rm UERS}(\nu_2)/T_{\rm UERS}(\nu_1)$. We have used this method in the same halo and disk regions used before. In this way we got values of $\overline{T_{\rm CMB}}$ in agreement with the results obtained by the PDT method. However, (1) we cannot separate the CMB temperature at the two frequencies and (2) there is an unfavorable combination of systematics on the zero-level assessment at the two frequencies:

$$\Delta T^{\rm CMB}_{\rm zero} = \left|\frac{m}{m-1}\right|\Delta T^{\rm sky}_{\rm zero}(\nu_1) + \left|\frac{1}{m-1}\right|\Delta T^{\rm sky}_{\rm zero}(\nu_2), \quad (9)$$

which, applied to TRIS data at $\nu_1 = 0.60$ and $\nu_2 = 0.82$ GHz, gives $m \simeq 0.38$–0.42 and $\Delta T^{\rm CMB}_{\rm zero} = ^{+0.76}_{-0.54}$ K. In order to avoid these limitations, we need to consider differences between pairs of positions in the sky. But in this case the set of equations we get is equivalent to the PDT method described above.

3.2. *Analysis of the Measurements at* 2.5 GHz

At 2.5 GHz no profile of $T_{\rm sky}$ versus α was available. Therefore, we were forced to adopt a more straightforward but less accurate method: evaluating $T_{\rm Gal}$ at $\nu = 2.5$ GHz from independent measurements, by a model, and subtracting it from $T_{\rm sky} - T_{\rm UERS}$ to

TABLE 6

BRIGHTNESS TEMPERATURE OF THE GALAXY AROUND THE MINIMUM AND THE MAXIMUM, RESPECTIVELY, AS MEASURED BY TRIS ANTENNAS AT $\delta = +42^\circ$

R.A. (h)	$T^{\rm TRIS}_{\rm Gal}$ (K) 0.60 GHz	$T^{\rm TRIS}_{\rm Gal}$ (K) 0.82 GHz	β
10.0 (halo)	5.72 ± 0.07	2.21 ± 0.03	3.09 ± 0.15
20.4 (disk)	24.44 ± 0.07	10.38 ± 0.03	2.76 ± 0.10

TABLE 7
BRIGHTNESS TEMPERATURE OF CMB AT 2.5 GHz

ν (GHz)	T_{CMB} (K)	ΔT_{zero} (K)	ΔT_{stat} (K)	ΔT_{Gal} (K)	ΔT_{UERS} (K)
2.50.....	2.458	0.284	0.103	0.093	0.001

NOTES.— The error budget due to the different contributions is quoted separately. Due to the small number of independent measurements, the statistical uncertainty of the experimental points is not negligible.

get T_{CMB}. We got T_{Gal} extrapolating data from the map of the diffuse radiation at 1.42 GHz prepared by Reich & Reich (1986), which is the one in the literature closest to $\nu = 2.5$ GHz, covering the sky region scanned by TRIS. This map has been convolved with the beam of the TRIS antennas in order to get the synthetic drift scan at $\delta = +42^\circ$. Then we extrapolated this signal at 2.5 GHz using the spectral index β calculated from TRIS data at 0.60 and 0.82 GHz (see Paper III). Finally, we subtracted T_{Gal} and T_{UERS} from T_{sky} and got T_{CMB}. The results are reported in Table 7. Here the statistical uncertainty on the experimental points ($\Delta T_{stat} =$ 103 mK) is larger than at lower frequencies because we have few independent measurements.

3.3. *Results*

The values of T_{CMB} obtained above, using different methods, are consistent within the error bars (see § 3.1). This means that the errors (statistics and systematics), proper of the measurements and arising from the analysis, are well represented by the quoted uncertainty (see Table 5).

The brightness temperatures of the CMB [$T_{CMB}(\nu)$] are converted into thermodynamic blackbody temperature [$T^{th}_{CMB}(\nu)$]:

$$T^{th}_{CMB}(\nu) = \frac{h\nu}{k \ln(x_b + 1)}, \qquad (10)$$

where $x_b = h\nu/kT_{CMB}$. Results are summarized in Table 8 and Figure 5 together with the results from previous measurements (see Table 1).

4. DISCUSSION

4.1. *Comparison with the Previous Measurements*

The results obtained by the TRIS experiment represent a significant improvement in the CMB measurements at frequencies lower than 1 GHz. If one excludes the two measurements made at the beginning of the 1990s (Sironi et al. 1990, 1991), all the remaining data were obtained before 1970.

Above 1 GHz in literature there are more accurate and recent results. These measurements give temperatures of the CMB that, within the error bars, are in agreement with the temperature measured by FIRAS at much higher frequencies. The only exceptions

TABLE 8
THERMODYNAMIC TEMPERATURE OF CMB AT 0.60, 0.82, AND 2.5 GHz

ν (GHz)	T^{th}_{CMB} (K)	ΔT_{zero} (K)	σ (K)
0.60.....	2.837	0.066	0.129
0.82.....	2.803	$^{+0.430}_{-0.300}$	0.051
2.50.....	2.516	0.284	0.139

NOTE.— Systematic and combined statistic (1 σ) error bars are quoted separately.

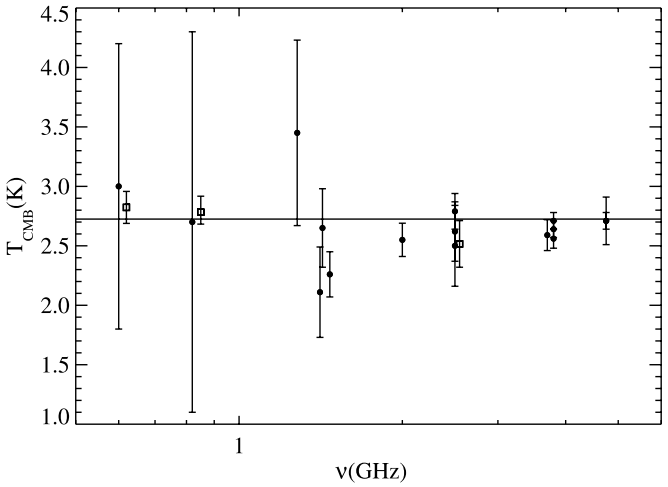

FIG. 5.— CMB thermodynamic temperature measured at low frequencies (see Table 1). For easier comparison with previous measurements (*filled circles*), TRIS data points (*open squares*) have been slightly shifted in frequency. The horizontal solid line is the CMB temperature obtained by FIRAS at higher frequencies.

are the results obtained at 1.4 GHz by Levin et al. (1988) and Bensadoun et al. (1993). It is hard to fit these results only with the spectral distortions allowed by *COBE* FIRAS (see Fixen et al. 1996).

Among the more recent experiments, the most promising program is ARCADE (see Kogut 2003). At the frequencies $\nu = 10$ and 30 GHz ARCADE has obtained results with error bars of 10 and 32 mK, respectively (see Fixen et al. 2004), which at 8.0 and 8.3 GHz go up to 120 and 160 mK, respectively (see Singal et al. 2006). The lowest frequency scheduled by ARCADE is 3.3 GHz. Unfortunately, above 2–3 GHz an accuracy of a few millikelvin is necessary to detect or further constrain the limits on distortions produced by Comptonization, BE, or FF processes, set by FIRAS. The search for BE and FF distortions is better done below 2–3 GHz. Here, in fact, larger distortions can be expected.

We can summarize our results in the following way:

1. At $\nu = 0.60$ GHz we reduced the error bar by a factor of ~9. Before TRIS the error bar was equally distributed between uncertainties on the temperature of the sky and uncertainties on the level of the Galactic and extragalactic foregrounds (see Sironi et al. 1990). The better accuracy of TRIS is due to improvement of the experimental setup and a better procedure of foreground subtraction.
2. At $\nu = 0.82$ GHz the error bar reduction resulting from TRIS is a factor of ~7. Due to the failure of the calibrator, TRIS results are still dominated by the systematic uncertainty on the zero level, while the error bar due to the foreground separation is smaller.
3. The TRIS measurement at $\nu = 2.5$ GHz does not improve but is fully compatible with the previous results (see Table 1). Combined with all the observations in literature, we get the value $T^{th}_{CMB}(2.5\ \text{GHz}) = 2.680 \pm 0.110$ K.

4.2. *The Spectral Distortions*

We can now combine TRIS results with the data in literature and look for better limits on spectral distortions. The Compton distortions are important only in the Wien region of the CMB spectrum. Therefore, in the following discussion we do not consider them.

The BE distortion is, conversely, important at frequencies lower than 1 GHz. Various analyses suggest that it can produce a dip in the brightness temperature at sub-GHz frequencies (see Burigana

et al. 1995; Burigana & Salvaterra 2003). The minimum is expected at a frequency

$$\nu_{\rm min}^{\rm BE} \propto \left(\Omega_b h^2\right)^{2/3}, \tag{11}$$

where Ω_b is the baryon density and h is the Hubble constant parameter. Assuming the *WMAP* results for $\Omega_b h^2$ (see Spergel et al. 2007), we expect $\nu_{\rm min}^{\rm BE} \sim 0.3$–$0.4$ GHz. Detection of $\nu_{\rm min}^{\rm BE}$ should give an independent estimate of the baryon density Ω_b. The dip amplitude is related to the chemical potential μ, by $\Delta T_{\rm BE} \propto \mu(\Omega_b h^2)^{-2/3}$. The limit set by *COBE* FIRAS on the chemical potential ($|\mu| < 9 \times 10^{-5}$) implies a spectral distortion $\Delta T_{\rm BE} \lesssim 17$ mK (95% CL), so the current measurements at low frequency, including TRIS, are not yet accurate enough to detect $\nu_{\rm min}^{\rm BE}$ and constrain further Ω_b.

The FF emission is expected to produce a temperature deviation with a quadratic dependence on the wavelength:

$$\Delta T_{\rm ff} = T_0 \frac{Y_{\rm ff}}{x^2}, \tag{12}$$

where $Y_{\rm ff}$ is the optical depth to FF emission and x is the dimensionless frequency (see Bartlett & Stebbins 1991). This kind of distortion is expected in the case of reionization of the intergalactic medium (IGM). The amplitude of the cosmological signal depends on the integrated column density of ionized gas produced at the redshift of formation of the first collapsed objects (Kogut 2003) and on the thermal history of the IGM through the electrons' temperature $T_e(z)$. The current upper limit set by the previous measurements at low frequency is $|Y_{\rm ff}| < 1.9 \times 10^{-5}$ (Bersanelli et al. 1994). A lower limit can be set by the observed Lyα forest: $|Y_{\rm ff}| \gtrsim 8 \times 10^{-8}$ and $\Delta T_{\rm ff} \gtrsim 2$–$3$ mK at $\nu = 0.6$ GHz (Haiman & Loeb 1997). A distortion $\Delta T_{\rm ff} \sim 30$ mK at $\nu = 0.6$ GHz, corresponding to $|Y_{\rm ff}| \sim 1.3 \times 10^{-6}$ due to a clumpy component from halos, has been suggested by Oh (1999). Moreover, several reionization models have been studied by Weller et al. (1999), where values of $|Y_{\rm ff}| \sim (0.5$–$4) \times 10^{-8}$ are suggested for different scenarios.

Combining TRIS measurements and the data in literature, we get a data set that has been used to fit the distorted (FF+BE) spectra of $T_{\rm CMB}$. It includes all the measurements reported in Table 1, plus the *COBE* FIRAS data (Fixen et al. 1996) and the measurements made by ARCADE (Fixen et al. 2004; Singal et al. 2006). We have combined the uncertainties of TRIS data assuming for the statistical one (σ) a normal distribution and for the systematic one ($\Delta T_{\rm zero}$) a uniform distribution. We set new limits to the FF effect: $-6.3 \times 10^{-6} < Y_{\rm ff} < 12.6 \times 10^{-6}$ at 95% CL. We also improved marginally the upper limits to BE distortions: $|\mu| < 6 \times 10^{-5}$ at 95% CL. The undistorted blackbody temperature has also been fitted, and we have confirmed, as expected, the results obtained by Fixen & Mather (2002). In Figure 6 we show the maximum frequency distortions, due to the FF effect, allowed after the present analysis. As clearly shown in Figure 6, the major improvement in the upper limits of $Y_{\rm ff}$ is due to the TRIS measurements, in particular the one at 0.60 GHz. The limits on $Y_{\rm ff}$ cover positive and negative values. The sign depends on the difference between the electron temperature T_e in the ionized medium and the radiation temperature T_γ. Mechanisms of recombination cooling can in fact lower the electron temperature down to $T_e \gtrsim 0.2 T_\gamma$, corresponding to $Y_{\rm ff} \gtrsim -2.3 \times 10^{-5}$ (see Stebbins & Silk 1986).

4.3. *Accuracy and Perspectives*

The total error budget of the CMB temperature measured by TRIS can be roughly separated into two blocks: uncertainty in the absolute measurements ($\Delta T_{\rm zero}$) and uncertainty due to the procedure of foreground subtraction (σ). For TRIS data at 0.60 and 0.82 GHz the statistics is not the dominant source of uncertainty. At 2.5 GHz the results are limited also by the statistics.

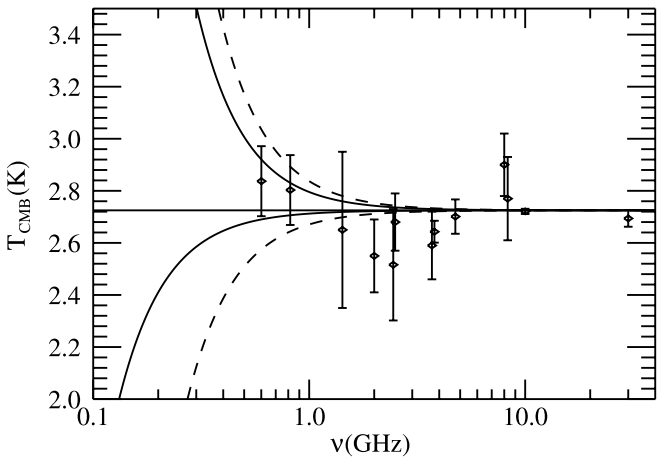

FIG. 6.—Distorted spectra due to the FF effect and measured CMB temperatures. Short-dashed lines correspond to 1 σ upper limits, while long-dashed lines correspond to 2 σ upper limits (95% CL). The solid line shows the undistorted CMB temperature. Measurements at the same frequencies have been combined in this plot. Here we report the error bars quoted in literature for the various experiments. TRIS data error bars (1 σ) result from the combination of statistical and systematic uncertainties.

Systematic uncertainties on the zero level are set by the capability of controlling and measuring losses and temperatures of the front-end components. As discussed in Paper I, at 0.60 GHz we get an accuracy $\Delta T_{\rm zero} = 66$ mK, a value achievable also at 0.82 GHz (we could not reach it due to the failure of the cryogenic system).

The evaluation of the foregrounds and their subtraction from $T_{\rm sky}$ is the other main source of uncertainty. The UERS brightness temperature can be evaluated by analyzing the number count measurements available in the literature (see Gervasi et al. 2008). Improvements on this value can only come from better source count measurements. The Galactic emission has been obtained as a by-product of TRIS observations by the TT-plot method, a technique that works properly if the signals are taken by identical instruments at different wavelengths. The use of existing maps is hampered by intercalibration problems, pointing errors, beam shape accuracy, etc. Minor sources of uncertainty are the atmospheric and ground contribution to the antenna temperature. These terms can be controlled by a proper design of the experiment.

We estimate that the best accuracy achievable at TRIS frequencies for $T_{\rm CMB}$, using the TRIS methods, is $\Delta T_{\rm tot} \sim 100$ mK. Better results require one to cool down the full front end, including the horn, and use a cryogenic calibrator in front of it. This is the strategy adopted by ARCADE, but this experiment is limited to frequencies $\nu \gtrsim 3$ GHz (see Fixen et al. 2004; Singal et al. 2006). Probably multifrequency space experiments at long wavelengths (see, for example, proposals like LOBO [Sironi et al. 1995, 1997] and DIMES [Kogut 1996]), taking advantage of the very stable conditions available in space, should allow us to bring $\Delta T_{\rm tot}$ below 100 mK also at frequencies lower than 1 GHz.

5. CONCLUSIONS

Starting from the absolute measurements of the sky brightness temperature, performed by the TRIS experiment and presented in Paper I, we have evaluated the absolute temperature of the CMB at $\nu = 0.60$, 0.82, and 2.5 GHz.

The thermodynamic temperatures of the CMB we get are $T^{\rm th}_{\rm CMB} = 2.837 \pm 0.129 \pm 0.066$ K at $\nu = 0.60$ GHz, $T^{\rm th}_{\rm CMB} = 2.803 \pm 0.051^{+0.430}_{-0.300}$ K at $\nu = 0.82$ GHz, and $T^{\rm th}_{\rm CMB} = 2.516 \pm 0.139 \pm 0.284$ K at $\nu = 2.5$ GHz. The first error bar is 1 σ statistics, while the second one is the systematic on the zero-level assessment.

Thanks to improvements of the absolute calibration system and in the foreground separation technique, TRIS succeeded in reducing previous uncertainties by a factor of $\sim$9 at $\nu = 0.60$ GHz and by a factor of $\sim$7 at $\nu = 0.82$ GHz. At 2.5 GHz TRIS results are in agreement with the previous measurements.

These results, used to look for CMB spectral distortions, give an upper limit to the chemical potential $|\mu| < 6 \times 10^{-5}$ (95% CL) used to describe the BE distortions. We have also constrained the FF distortions to $-6.3 \times 10^{-6} < Y_{\rm ff} < 12.6 \times 10^{-6}$ (95% CL), approaching the values suggested by observations of the Lyα forest (Haiman & Loeb 1997).

The TRIS activity has been supported by MIUR (Italian Ministry of University and Research), CNR (Italian National Council of Research), and the Universities of Milano and of Milano-Bicocca. The logistic support at Campo Imperatore was provided by INFN, the Italian Institute of Nuclear Physics, and its Laboratorio Nazionale del Gran Sasso. The authors acknowledge also an anonymous referee for his comments that helped us to improve the quality of the results presented.

REFERENCES

Ajello, C., Bonelli, G., & Sironi, G. 1995, ApJS, 96, 643
Bartlett, J. G., & Stebbins, A. 1991, ApJ, 371, 8
Bennet, C. L., et al. 1996, ApJ, 464, L1
Bensadoun, M., et al. 1993, ApJ, 409, 1
Bersanelli, M., et al. 1994, ApJ, 424, 517
Burigana, C., Danese, L., & De Zotti, G. 1991a, A&A, 246, 49
Burigana, C., De Zotti, G., & Danese, L. 1991b, ApJ, 379, 1
———. 1995, A&A, 303, 323
Burigana, C., & Salvaterra, R. 2003, MNRAS, 342, 543
Daly, R. A. 1991, ApJ, 371, 14
Davies, R. D., Watson, R. A., & Gutiérrez, C. M. 1996, MNRAS, 278, 925
De Amici, G., et al. 1988, ApJ, 329, 556
———. 1990, ApJ, 359, 219
———. 1991, ApJ, 381, 341
Dubrovich, V. K., & Stolyarov, V. A. 1995, A&A, 302, 635
Fixen, D. J., Cheng, E. S., Gales, J. M., Mather, J. C., Shafer, R. A., & Wright, E. L. 1996, ApJ, 473, 576
Fixen, D. J., & Mather, J. C. 2002, ApJ, 581, 817
Fixen, D. J., et al. 2004, ApJ, 612, 86
Gervasi, M., Tartari, A., Zannoni, M., Boella, G., & Sironi, G. 2008, ApJ, 682, 223
Haiman, Z., & Loeb, A. 1997, ApJ, 483, 21
Illarionov, A. F., & Sunyaev, R. A. 1975a, Soviet Astron., 18, 413
———. 1975b, Soviet Astron., 18, 691
Kogut, A. 1996, preprint (astro-ph/9607100)
———. 2003, NewA Rev., 47, 945
Kogut, A., et al. 2004, ApJS, 154, 493
Levin, S. M., et al. 1988, ApJ, 334, 14
Mandolesi, N., Calzolari, P., Cortiglioni, S., & Morigi, G. 1984, Phys. Rev. D, 29, 2680
Mandolesi, N., et al. 1986, ApJ, 310, 561
Mather, J. C., Fixen, D. J., Shafer, R. A., Mosier, C., & Wilkinson, D. T. 1999, ApJ, 512, 511
Mather, J. C., et al. 1990, ApJ, 354, L37
Mather, J. C., et al. 1994, ApJ, 420, 439
Oh, S. P. 1999, ApJ, 527, 16
Platania, P., Bensadoun, M., Bersanelli, M., De Amici, G., Kogut, A., Levin, S., Maino, D., & Smoot, G. F. 1998, ApJ, 505, 473
Raghunathan, A., & Subrahmanyan, R. 2000, J. Astrophys. Astron., 21, 1
Reich, P., & Reich, A. 1986, A&AS, 63, 205
Singal, J., et al. 2006, ApJ, 653, 835
Sironi, G., Boella, G., Gervasi, M., Finocchiaro, G., & Attiná, P. 1997, in Proc. 48th International Astronautical Congress, IAF-97, q.1.08
Sironi, G., & Bonelli, G. 1986, ApJ, 311, 418
Sironi, G., Bonelli, G., Dall'Oglio, G., Pagana, E., De Angeli, S., & Perelli, M. 1995, Astrophys. Lett., 32, 31
Sironi, G., Bonelli, G., & Limon, M. 1991, ApJ, 378, 550
Sironi, G., Inzani, P., & Ferrari, A. 1984, Phys. Rev. D, 29, 2686
Sironi, G., Limon, M., Marcellino, G., Bonelli, G., Bersanelli, M., Conti, G., & Reif, K. 1990, ApJ, 357, 301
Spergel, D. N., et al. 2007, ApJS, 170, 377
Staggs, S. T., Jarosik, N. C., Wilkinson, D. T., & Wollak, E. J. 1996, ApJ, 458, 407
Stebbins, A., & Silk, J. 1986, ApJ, 300, 1
Sunyaev, R. A., & Zel'dovich, Ya. B. 1970, Ap&SS, 7, 20
———. 1980, ARA&A, 18, 537
Tartari, A., Zannoni, M., Gervasi, M., Boella, G., & Sironi, G. 2008, ApJ, 688, 32 (Paper III)
Turtle, A. J., Pugh, J. F., Kenderdine, S., & Pauliny-Toth, I. I. K. 1962, MNRAS, 124, 297
Varshalovich, D. A., & Khersonskii, V. K. 1977, Soviet Astron. Lett., 3, 155
Weller, J., Battye, R. A., & Albrecht, A. 1999, Phys. Rev. D, 60, 103520
Zannoni, M., Tartari, A., Gervasi, M., Boella, G., Sironi, G., De Lucia, A., Passerini, A., & Cavaliere, F. 2008, ApJ, 688, 12 (Paper I)
Zel'dovich, Ya. B., Illarionov, A. F., & Sunyaev, R. A. 1972, Soviet Phys.-JETP, 35, 643
Zel'dovich, Ya. B., & Sunyaev, R. A. 1969, Ap&SS, 4, 301